



Morphology, Microstructure and Improved Mechanical Properties of $\text{TiB}_2/\text{TiB}/\text{TiN}$ Reinforced Ti_3Al Matrix Composite Coating with ZrO_2 Addition

Xinmeng Sui¹ · Jian Lu¹ · Weiping Zhang¹

Submitted: 24 June 2019 / in revised form: 14 January 2020 / Published online: 23 January 2020
© ASM International 2020

Abstract Ti_3Al matrix composite coatings were synthesized on a TC4 titanium alloy with Ti, Al and BN mixed powder by in situ laser cladding. Then, the effect of ZrO_2 addition to the composite coatings was investigated. The phase composition, microstructure and element distribution of the composite coatings were characterized by scanning electron microscopy, x-ray diffraction and electron probe microanalysis. Results showed that the Ti_3Al matrix composite coatings were reinforced by TiB_2 , TiB and TiN phases. The quality and mechanical properties of the composite coating can be significantly improved with ZrO_2 addition under optimum laser power of 1000 W. The microhardness of the composite coatings was 2–3 times higher than that of the substrate, and the wear resistance of the composite coating without and with ZrO_2 addition was enhanced by nearly 4 and 7 times compared to the substrate. The better properties of the composite coating with ZrO_2 addition were mainly attributed to the formation of a ZrO_2 network. The network-like distribution of ZrO_2 provided dispersion strengthening and grain refinement effects. This research is expected to provide a new coating material to obtain high-performance Ti_3Al matrix composite coating.

Keywords laser cladding · microstructure · Ti_3Al matrix composite coating · wear resistance · ZrO_2

Introduction

Titanium and its alloys have emerged as indispensable structural components for various applications such as aviation, aerospace, weapon and automobile manufacturing due to their high specific strength and exceptional corrosion resistance (Ref 1–4). Nevertheless, the utilization of titanium alloys in transmissions and under sliding contact conditions is restricted owing to their low hardness and insufficient wear resistance (Ref 5–7). In order to overcome these shortcomings, surface modification with laser techniques were widely utilized; in particular, the laser cladding surface modification of titanium with an appropriate coating has been extensively applied in recent years (Ref 8–10). Moreover, numerous studies indicated that ceramic-reinforced composite coatings with metal or metal alloy matrix are the most desirable material system. In this composite system, ceramics act as reinforcing phases, metals or alloys serve as the binder phases, so that the synthesized composite coatings exhibit good mechanical properties with proper process parameters (Ref 11, 12).

Recently, ceramic particles-reinforced Ti_3Al matrix composite coatings have been widely fabricated on titanium alloy by in situ laser cladding, owing to their favorable compatibility with titanium alloy substrate and good wear resistance (Ref 13, 14). Feng et al. (Ref 15) fabricated ($\text{Ti}_3\text{Al} + \text{TiB}$)/Ti composite coatings on Ti6Al4V substrates by in situ laser cladding process with mixed Ti and AlB₂ powder. The results showed that the average hardness of the composite coating increased significantly compared to the substrate because of dispersion strengthening and solid solution strengthening. The average wear loss of the coating was only 12.5% that of the substrate. Liu et al. (Ref 14) prepared a TiN/ Ti_3Al intermetallic compound composite coating with Ti and AlN mixed powder, and its

✉ Weiping Zhang
electron_beam@163.com

¹ Key Laboratory of Solidification Control and Digital Preparation Technology (Liaoning Province), School of Materials Science and Engineering, Dalian University of Technology, Dalian 116024, People's Republic of China

microhardness was 3 times higher than that of the Ti6Al4V titanium alloy substrate. In summary, nitrides and carbide ceramics were often added into Ti_3Al matrix to improve the properties of the composite coating, including TiC, SiC, WC, TiN and so on (Ref 16, 17).

However, defects identified as cracks, pores and inclusions are easily generated during laser cladding of Ti_3Al matrix composite coating. Various studies undertaken have concluded that the absorption of rare earth (RE) in the cladding material systems can reduce the dilution ratio (Ref 18–20), improve coating toughness (Ref 21, 22) and reduce cracking tendency (Ref 23–25). However, the RE was a non-renewable resource; careful selection and optimization of the added quantity are a prerequisite. By comparison, the easily accessible oxide ceramic ZrO_2 has excellent high temperature strength, high hardness and wear resistance (Ref 26, 27). It also has the effect of eliminating the defects and refining the microstructure of coatings produced by laser cladding. Therefore, the addition of ZrO_2 ceramic reinforcing phase to Ti_3Al matrix composite coating is a potential method to reduce cracks and improve the hardness and wear properties. Moreover, there is no clear report on the enhancement effect of ZrO_2 on Ti_3Al matrix composite coating by in situ laser cladding.

In this study, a new laser cladding material system consisting of Ti, Al and BN mixed powders was used to fabricate Ti_3Al matrix composite coating by in situ laser cladding. The laser power was optimized, and phase composition and microstructure evolution of the composite coatings with and without ZrO_2 addition were investigated; the effect of ZrO_2 addition on the properties of the composite coatings was studied, and the microhardness and wear resistance of the composite coatings were preliminarily discussed.

Materials and Experimental Methods

In this experiment, a commercial TC4 titanium alloy was used as the substrate material, and its chemical composition is given in Table 1. Rectangular specimens with dimension 30 mm × 15 mm × 8 mm were cut by a milling machine. The substrate was ground to achieve a surface roughness ~ 1.6 μm by mechanical polishing and then cleaned with anhydrous ethanol and acetone. Commercially pure Ti powder (99.6% purity, 75–90 μm), Al

powder (99.9% purity, 75–90 μm), pure BN powder (99.9% purity 2–5 μm) and ZrO_2 powder (99.9% purity, 1–3 μm) provided by Liaoning ZhongSe New Materials Technology Co., Ltd (Liaoning, China) were selected as the laser cladding materials. The experiment adopted pre-placed powder method and single-pass cladding. The mixed powders were homogeneously ground in an agate mortar and then pre-placed on the substrate surface by an organic binder (5% polyvinyl alcohol solution) in a mass ratio of 5:1 with a thickness of 2.0 mm. Then, the pre-placed coatings were dried using a drying cabinet at room temperature.

The laser cladding experiment was carried out on TC4 alloy by a continuous semiconductor laser, which was a laserline LDF 4000–100 with a six-joint robot manipulator, and the wavelength was 900 nm. The schematic of the laser cladding process is shown in Fig. 1. Argon was blown into the molten pool as shielding gas with a pressure of 0.2 MPa to prevent oxidation during laser cladding. In order to determine the optimal laser power, laser cladding specimens numbered from specimen 1 to 5 (without ZrO_2), all with molar ratios of 8Ti:6Al:3BN, were fabricated under specific cladding parameters listed in Table 2. Then, a specimen with molar ratios of 8Ti: 6Al: 3BN: 1ZrO₂ was prepared through the optimum laser power and numbered specimen 6.

After laser cladding, the specimens were sectioned perpendicularly to the scanning direction by wire electrical discharge machining cutting. Metallographic specimens were prepared using standard mechanical polishing procedures and were chemically etched in a solution of HF,

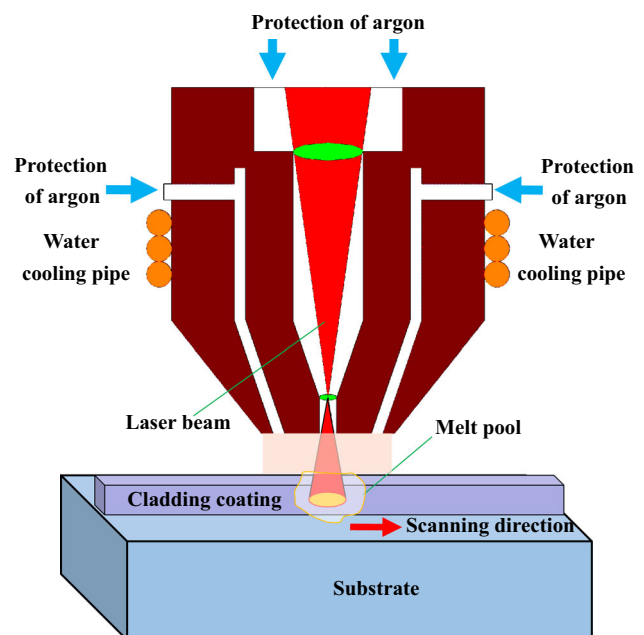


Fig. 1 Schematic of the laser cladding process

Table 1 Chemical composition of the TC4 titanium alloy (wt.%)

Ti	Al	V	Fe	C	O	N	H
Bal	5.5–6.8	3.5–4.5	0.3	0.1	0.2	0.05	0.015

Table 2 Parameters of the laser cladding process in the experiment

Number	Laser power, W	Scanning speed, mm/s	Spot diameter, mm
Specimen 1	900	5	3
Specimen 2	1000	5	3
Specimen 3	1100	5	3
Specimen 4	1200	5	3
Specimen 5	1300	5	3

HNO₃ and H₂O in volume ratio of 2:1:12 at room temperature for approximately 50 s.

The dilution ratio η is an important factor affecting the performance of cladded coatings, and is commonly calculated by Eq 1:

$$\eta = h/(h + H) \quad (\text{Eq 1})$$

where h is the molten depth of substrate, H is the thickness of the composite coatings, and the corresponding dimensions are measured using Image Pro Plus image processing analysis software.

The phase composition of the cladded coatings was examined using an XRD-6000 x-ray diffractometer with Co K α radiation at 40 and 40 mA by scanning an angular range from 20° to 100°. The microstructure of the cladded coatings was characterized using Zeiss Supra55 scanning electron microscope (SEM). The element distribution was evaluated with an electron probe microprobe analyzer (EPMA-1600). Dye penetration test was applied to identify the number of defects including cracks and holes on the cross section of the cladded coatings, the experimental details were based on the standard ASTM E165. A Vickers microhardness tester (DHV-1000) was employed to measure the microhardness profile of the coating along the depth direction with a load of 9.8 N and duration 15 s. Three points were measured at each position, and the average of the three points was taken as the microhardness value. A CFT-I comprehensive friction wear tester (CFT-I) was employed to identify the wear resistance of the substrate and cladded coatings, using a reciprocating sliding mode; the counterpart was a Si₃N₄ ball with a diameter of 3 mm, and the sliding speed was 200 mm/min at a load of 10 N for a duration of 40 min. The ball counterpart would be replaced after every sliding test.

Results and Discussion

Optimization of the Laser Power

Figure 2 shows the cross-sectional microstructures of composite coatings obtained under different laser powers. Specimen 1 exhibited some holes and unmelted particles as shown in Fig. 2(a). This was attributed to the insufficient

laser power; unmelted particles stayed in the molten pool, forming inclusions and holes. As the power increased, the unmelted particles gradually dissolved until they disappeared completely. However, with increased power, cracks were generated in the bonding zone of specimens 4 and 5 as shown in Fig. 2(d) and (e), and the greater the power, the larger the cracks. Overheating of the system leads to excessive residual stress in the coating, which was the main reason of the cracks (Ref 28). Additionally, the dilution ratio was an important factor affecting the quality of the coating; dilution ratios were 12.6, 13.7, 15.1, 18.9 and 21.0% for specimens 1-5, i.e., dilution increased with laser power. Overheating of specimens 4 and 5 by the laser led to excessive dilution of the coating by the substrate, thus resulting in increased possibility of coating cracking and in a deterioration of the coating performance such as hardness and wear resistance (Ref 29). The average hardness and the number of defects in specimens 1-5 are shown in Fig. 3. By combining Figs. 2 with 3, it is inferred that when the laser power was 1000 W, the cladding layer of specimen 2 has the best quality, the lowest number of defects and the highest hardness with dilution ratio 13.7%. Then, specimens 2 and 6 were characterized further to investigate how the properties of the composite coating are changed by the addition of ZrO₂.

Phase Analysis

X-ray diffraction (XRD) patterns corresponding to cladded specimens 2 and 6 are shown in Fig. 4. The composite coatings mainly consist of Ti₃Al, TiB₂, TiB, TiN and Ti phases. Under heating by the high-energy laser beam, the cladding materials and a thin surface layer of the substrate melted rapidly and the molten pool formed (Ref 30, 31). Subsequently, complicated reactions occurred in the molten pool, and various phases emerged as mentioned above. Based on the XRD results, it can be interpreted that the dominant phase was Ti₃Al. Moreover, a portion of the BN phase dissolved owing to the high temperature induced by irradiating the powder with the laser beam, thus resulting in delivering B and N elements in the molten pool. Chemical reactions then occurred between the diffused B/N and titanium due to their high affinity.

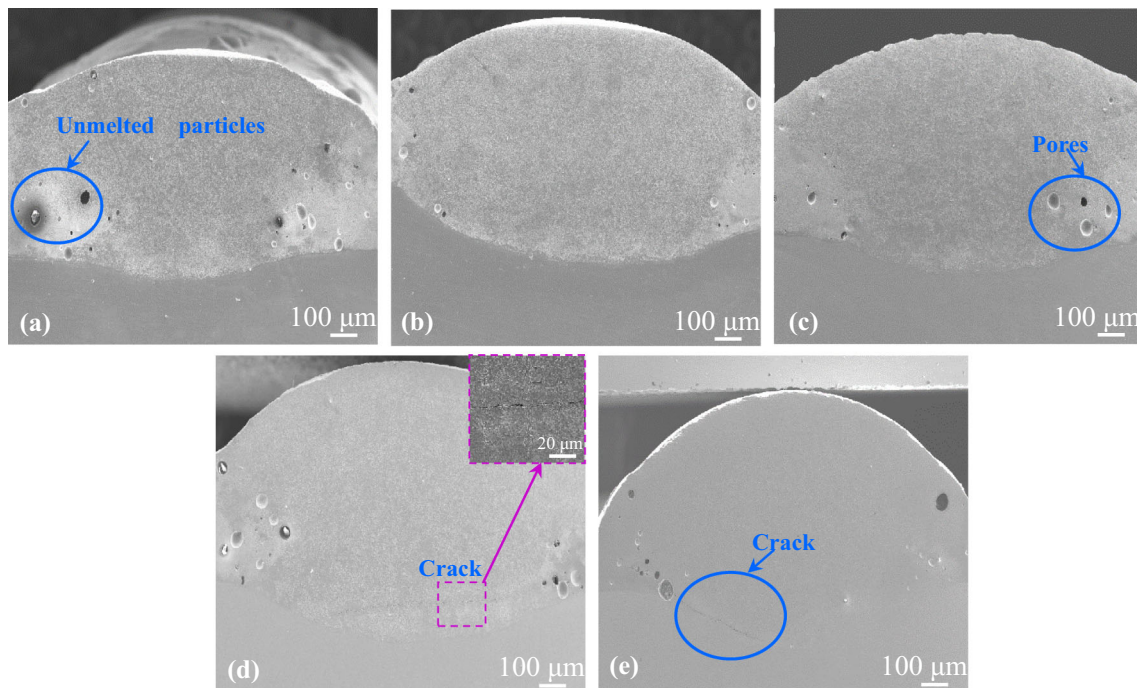


Fig. 2 Overview of the cross-sectional microstructure of the composite coatings in (a) specimen 1, (b) specimen 2, (c) specimen 3, (d) specimen 4 and (e) specimen 5

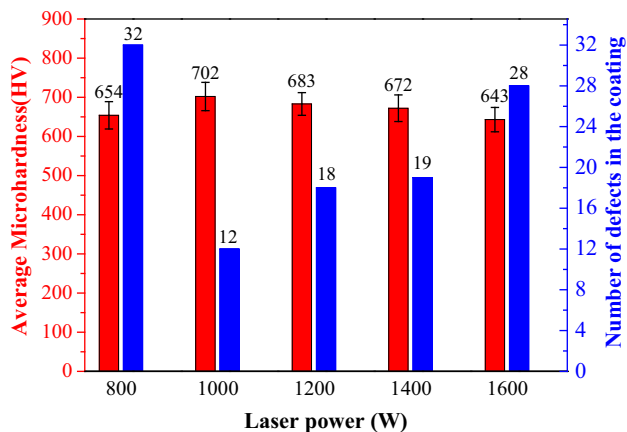
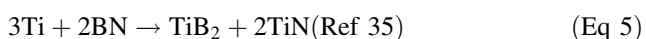


Fig. 3 Average hardness and the number of defects in specimens 1-5

The main chemical reactions generated in the molten pool were characterized as follows:



It was worth noting that the peaks of m-ZrO₂ and t-ZrO₂ phases were also observed in the coating of specimen 6, and no other phases were detected because of the addition of ZrO₂. Zirconia (ZrO₂) has a high melting temperature (2527 °C) and exists in three different forms (Ref 36).

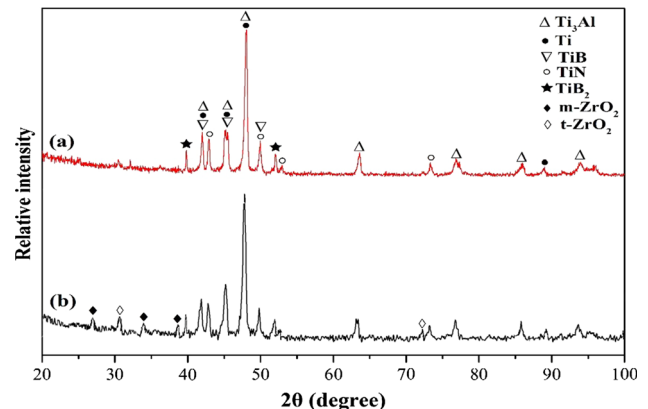


Fig. 4 XRD patterns corresponding to cladded coatings (a) specimen 2, (b) specimen 6

Phase transformation of ZrO₂ ceramic occurred during the cooling process. At high temperatures, it crystallizes in the cubic crystal structure (above 2370 °C), the tetragonal phase (t-ZrO₂) appears in the middle temperature range (1170-2370 °C), and when the temperature falls below 1170 °C, the tetragonal phase (t-ZrO₂) transforms to monoclinic phase (m-ZrO₂) (Ref 37, 38). The original ZrO₂ powder consisted of m-ZrO₂ phase, but the cladded coating consisted of m-ZrO₂ and t-ZrO₂ phases. This can be explained by the rapid heating and cooling process during laser cladding. The high cooling rate restrained the t-ZrO₂ transformation to m-ZrO₂ phase, so a small portion of t-ZrO₂ phase remained at ambient temperature (Ref 39).

Microstructure Characterization

Figure 5 shows the cross-section morphologies of specimens 2 and 6, respectively. Dense and compact coatings were fabricated on the substrates. Some pores were apparently observed on the coating of specimen 2 (Fig. 5a), while only three pores were detected in specimen 6 by the dye penetration test; therefore, specimen 6 is comparatively defect-free (Fig. 5b). Obviously, the addition of a small amount of ZrO_2 can improve the quality of the composite coating obtained with an optimum laser power of 1000 W. Figure 5(c) and (d) presents detailed morphologies of the typical microstructure of the composite coating, where fishbone structure, and needle-like, rod-like and hexagonal like structures were observed. The fishbone structure of specimen 6 was finer compared to specimen 2. In addition, the typical morphologies of TiB and TiB_2 were

spotted out, respectively. Based on the previous research, TiB tends to grow into fine or dense needles (Ref 40), while TiB_2 preferentially grows into bulk or hexagonal plate-like structures (Ref 41). Moreover, the microstructure of the bonding area plays an important role on the mechanical properties of the coating (Ref 42); therefore, a closer observation was carried out for both specimens. Sound metallurgical bonds (the bonding zone) between the cladding zone and the substrate were attained for both specimens (Fig. 5e and f). However, the microstructure of the bonding zone in specimen 6 revealed much more refined features than that in specimen 2, an amount of fine particle-like reinforcements distributed evenly in the bonding zone (Fig. 5f). Furthermore, comparing Fig. 5(c) and (d) with (e) and (f), the amount of reinforcing phases decreased remarkably from the coating to the bonding zone.

Fig. 5 Cross-section morphologies of specimen 2 and 6. (c–f) are local magnified SEM micrographs of c–f areas as shown in (a) and (b), respectively

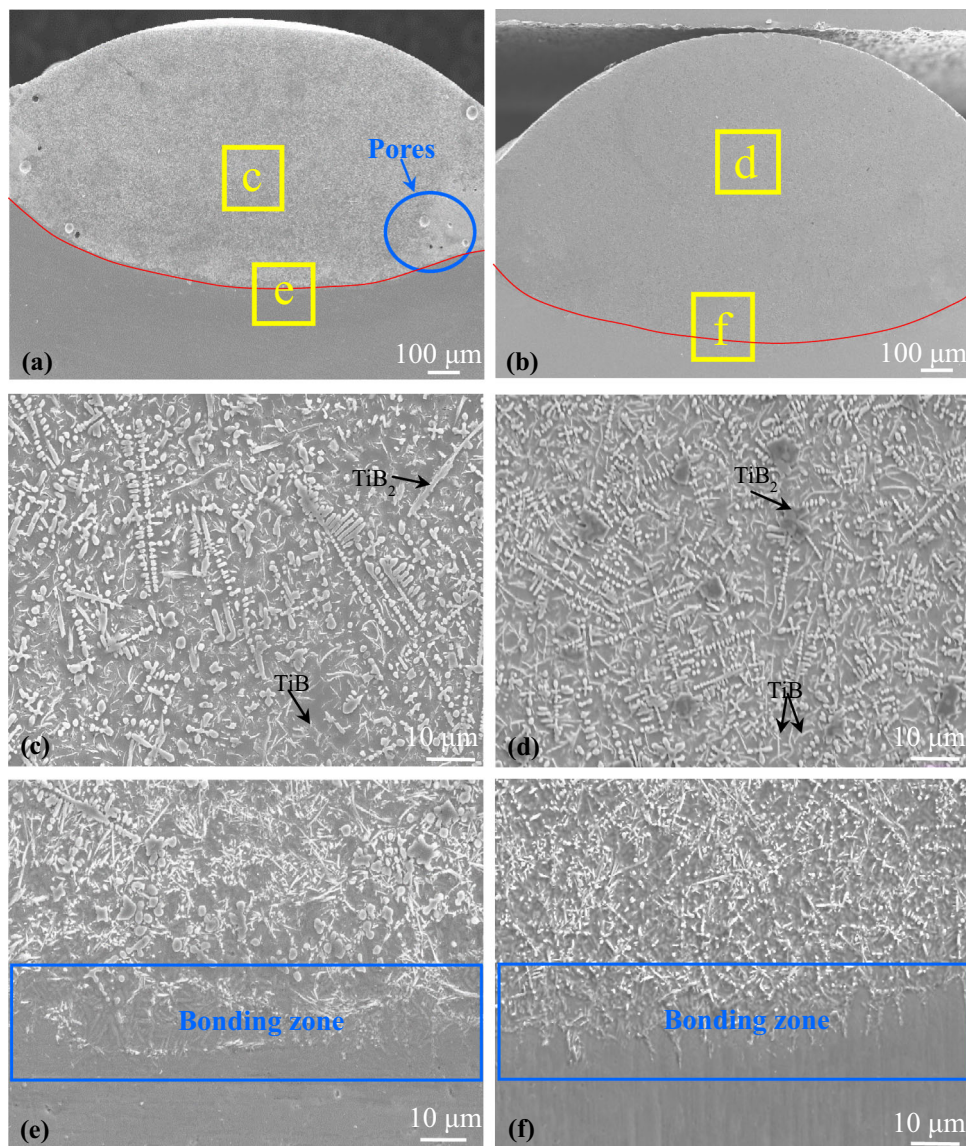
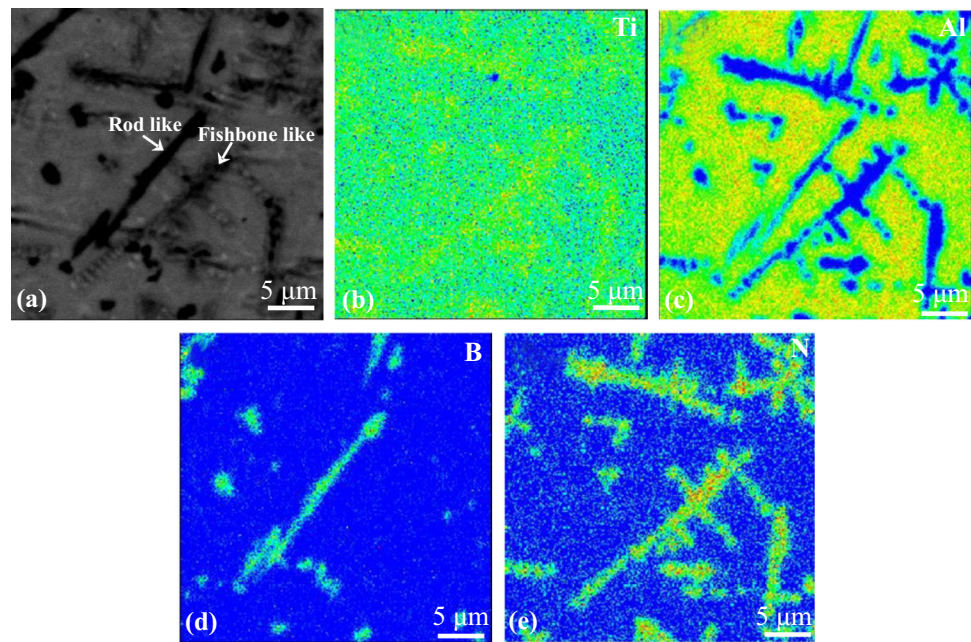


Fig. 6 EPMA image of the composite coating in specimen 2: (a) black scattered electron image, (b–e) corresponding elemental mapping of Ti, Al, B and N



In order to further distinguish the distribution of certain phases in the coatings, EPMA was implemented on specimens 2 and 6. Figures 6 and 7 show the microstructure of the coating with larger magnification compared to Fig. 5(c) and (d). On the one hand, combining the results of Fig. 6 and the XRD patterns, the composite coating of specimen 2 was composed of coarse TiN, TiB₂, TiB, Ti and Ti₃Al. As shown in Fig. 7(a), specimen 6 consists of a continuous matrix phase (marked A), black inclusions (marked B), black needles (marked C), gray-black dendrites (marked D) and white network-like features (marked E). The EPMA results are shown in Fig. 7(b), (c), (d), (e), and (f); combining the results of XRD, SEM and EPMA, the continuous matrix phase (marked A) was rich in Ti and Al, so it is identified as Ti₃Al. The black inclusion (marked B) and black needle (marked C) were abundant in B; accordingly, combined with the microstructure results of Fig. 5(d), the black inclusion (marked B) was TiB₂ and the black needle (marked C) was TiB. The gray-black dendrite (marked D) was TiN, and the white network-like feature (marked E) distributed across the matrix of Ti₃Al corresponded to ZrO₂. Combining the microstructural investigation and EMPA results of the coatings, the fishbone TiN microstructure of specimen 2 was coarser than specimen 6, and the TiB₂ microstructure changed from rod like to hexagonal like. The reasons were mainly attributed to two aspects. One is that ZrO₂ increased the nucleation rate during crystallization because of its high melting temperature and chemical inertness, resulting in increased nucleation rate and grain refinement. The other is that the network-like distribution of ZrO₂ inhibited the outward growth of the matrix grains, further exerting a grain

refinement action (Ref 43). Therefore, the addition of ZrO₂ can provide strengthening by grain refinement and also has an effect of dispersion strengthening for the composite coating. The composition and distribution of phases have a key influence on the hardness and wear resistance of the clad coating.

Microhardness and Wear Resistance

The microhardness distribution along the cross section of the clad coatings is shown in Fig. 8. It is evident that the two specimens showed similar microhardness trends. The microhardness of the coatings was 2–3 times higher than that of the TC4 substrate, which was ascribed to the comprehensive effects of Ti₃Al, TiB₂, TiB, TiN and ZrO₂ strengthening phases. However, the average microhardness of the coating on specimen 6 was higher than specimen 2. This was mainly attributed to the dispersion strengthening and grain refinement effect of the added ZrO₂. It can also be seen that the microhardness decreased as the testing point moved closer to the substrate; this phenomenon was strongly correlated with the distribution of hard phases across the coatings, which was observed in SEM micrographs. Together with the microstructure results discussed above, it is believed that a larger number of reinforcing second-phases lead to higher hardness (Ref 11).

Figure 9 shows the wear volume loss curves of the specimens. It can be seen that the wear volume loss of the substrate was significantly higher than that of the coatings. The wear volume loss of the substrate, specimens 2 and 6, was $2.69 \times 10^{-10} \text{ m}^3$, $0.65 \times 10^{-10} \text{ m}^3$, $0.4 \times 10^{-10} \text{ m}^3$, respectively. Hence, the wear resistance of specimens 2

Fig. 7 EPMA image of the composite coating in specimen 6: (a) black scattered electron image, (b–f) corresponding elemental mapping of Ti, Al, B, N, Zr and O

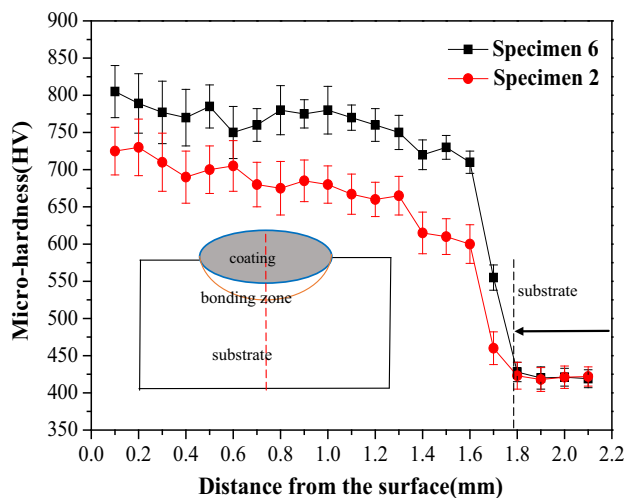
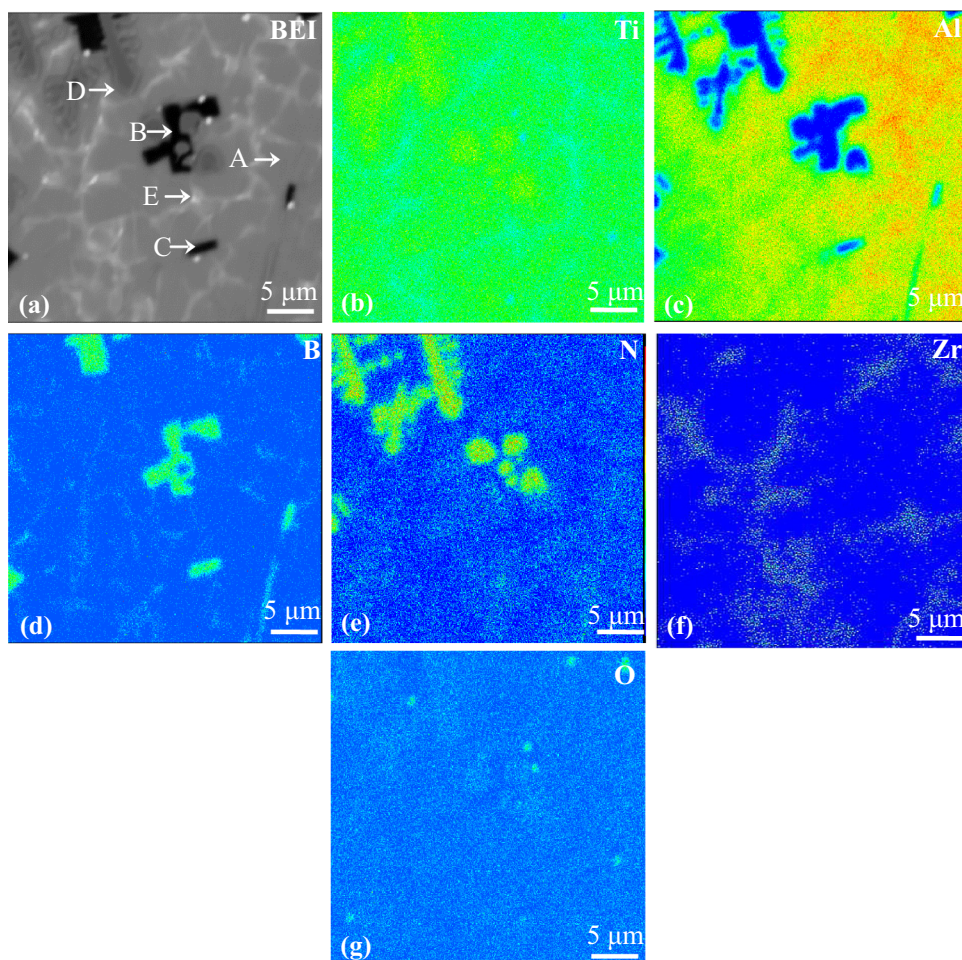


Fig. 8 Microhardness distributions along the cross section of the cladded coatings in specimens 2 and 6

and 6 was enhanced by nearly 4 and 7 times compared to the substrate. Furthermore, specimen 6 exhibited better wear resistance than specimen 2, corresponding to its

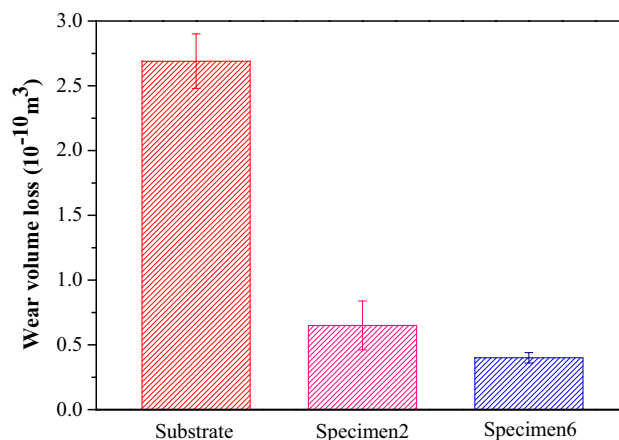
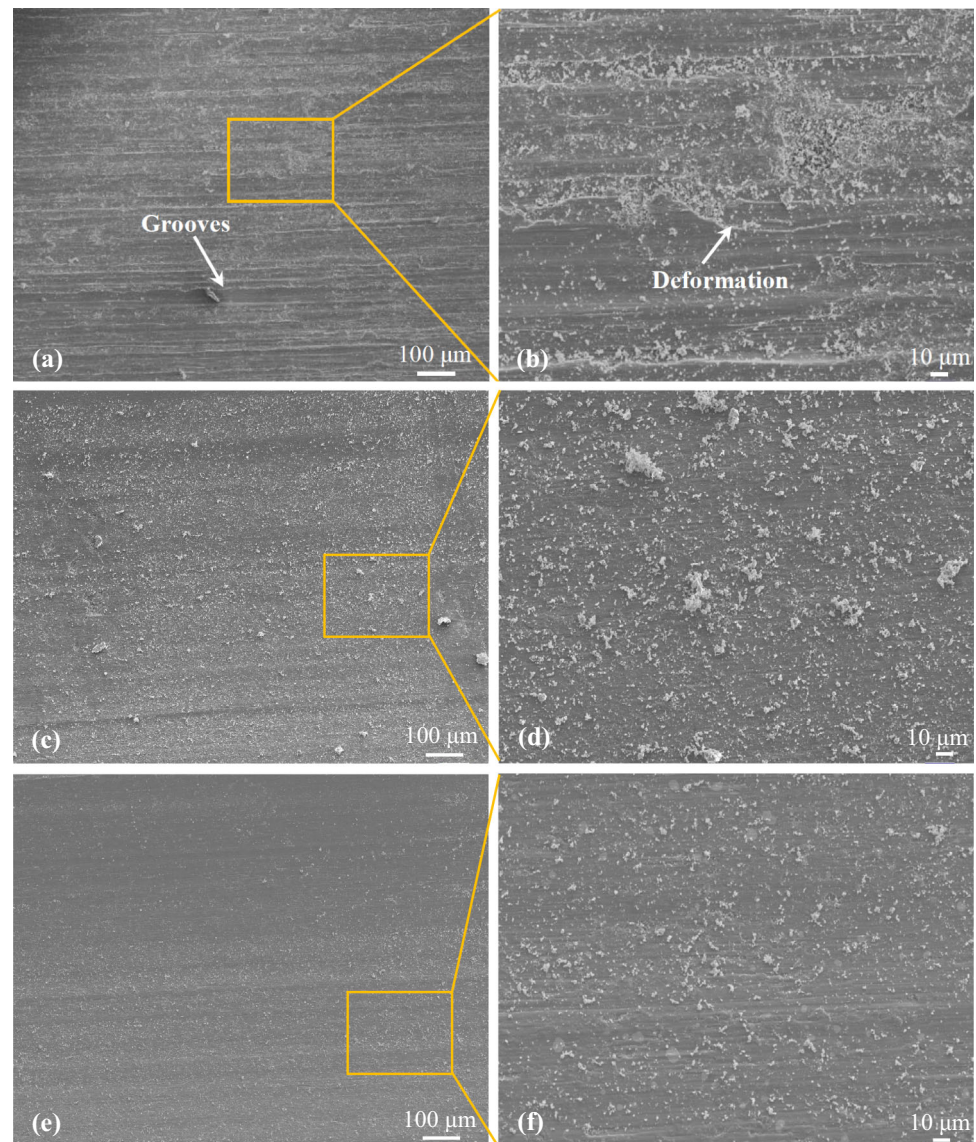


Fig. 9 Wear volume loss curves of the composite coatings

higher microhardness. The results were well-consistent with the microhardness distributions.

In order to understand the wear mechanisms of the substrate and coatings, their wear morphologies were characterized with SEM (Fig. 10). Results showed that the wear surface of the substrate was extremely coarse, with

Fig. 10 Worn surface morphologies of the substrate and composite coatings. (a, b) substrate, (c, d) specimen 2, (e, f) specimen 6



numerous spalling events. Serious plastic deformation features and grooves occurred, indicating that the worn surface of the substrate could easily undergo plastic deformation and grooving due to its low hardness. Subsequently, after a certain number of wear cycles, spallation was found to occur frequently on the wear surface of the substrate along grooves (Fig. 10a and b). Therefore, the wear mechanisms of substrate comprised adhesive and abrasive wear. On the other hand, the wear surfaces were smooth for both coatings with shallow plowing grooves (Fig. 10c and e), coupled with some debris particles. The shallow grooves were all parallel to the sliding direction, revealing a predominant abrasive wear mechanism. Moreover, it was apparent that the size of debris particles on specimen 6 was significantly smaller than it was on specimen 2. This was ascribed to the grain refinement and dispersion strengthening effect of the ZrO_2 addition.

Conclusions

In this study, Ti_3Al matrix composite coatings were fabricated on TC4 titanium alloy by in situ laser cladding. The effect of ZrO_2 addition on the microstructure and properties of Ti_3Al matrix composite coatings were investigated. The conclusions can be drawn as follows:

- (1) The composite coatings were mainly reinforced by TiB_2 , TiB and TiN phases.
- (2) The network-like distribution of ZrO_2 in the Ti_3Al matrix inhibits grain growth and plays the role of refining the microstructure of the coating.
- (3) The composite coating with ZrO_2 addition exhibited higher hardness and wear resistance than that without ZrO_2 under optimum laser power of

1000 W. This was attributed to the dispersion strengthening and grain refinement effect of ZrO₂.

- (4) The wear mechanisms of the substrate were adhesive and abrasive wear, and the wear mechanism of the composite coatings was mainly abrasive wear.

Acknowledgments This work was supported by the Natural Science Foundation of China under Grant Nos. 51471043 and the Aviation Industry Corporation Research Project (cxy2103DLLG34).

References

- C. Leyens and M. Peters, *Titanium and Titanium Alloys*, Wiley-VCH, Cologne, 2003
- E.O. Ezugwu and Z.M. Wang, Titanium Alloys and Their Machinability, *J. Mater. Process. Technol.*, 1997, **68**, p 262-274
- D. Carou, E.M. Rubio, J. Herrera, C.H. Lauro, J.P. Davim, D. Carou, E.M. Rubio, J. Herrera, C.H. Lauro, and J.P. Davim, Latest Advances in the Micro-Milling of Titanium Alloys: A Review, *Procedia Manuf.*, 2017, **13**, p 275-282
- N.W. Khun, A.W.Y. Tan, and E. Liu, Mechanical and Tribological Properties of Cold-Sprayed Ti Coatings on Ti-6Al-4V Substrates, *J. Therm. Spray Technol.*, 2016, **25**(4), p 715-724
- W. Zhang, Z. Zhu, and C.Y. Cheng, A Literature Review of Titanium Metallurgical Processes, *Hydrometallurgy*, 2011, **108**(3–4), p 177-188
- Y. Zhang, D. Sun, X. Gu, and H. Li, Strength Improvement and Interface Characteristic of Direct Laser Welded Ti Alloy/Stainless Steel Joint, *Mater. Lett.*, 2018, **231**, p 31-34
- J. Zhang, X. Li, D. Xu, and R. Yang, Recent Progress in the Simulation of Microstructure Evolution in Titanium Alloys, *Prog. Nat. Sci. Mater. Int.*, 2019, **29**(3), p 295-304
- B.A. Obadele, A. Andrews, P.A. Olubambi, M.T. Mathew, and S. Pityana, Effect of ZrO₂ addition on the Dry Sliding Wear Behavior of Laser Clad Ti6Al4 V Alloy, *Wear*, 2015, **328–329**, p 295-300
- F. Weng, C. Chen, and H. Yu, Research Status of Laser Cladding on Titanium and Its Alloys: A Review, *Mater. Des.*, 2014, **58**, p 412-425
- Q. Gao, H. Yan, Y. Qin, P. Zhang, J. Guo, and Z. Chen, Laser Cladding Ti-Ni/TiN/TiW + TiS/WS₂ Self-Lubricating Wear Resistant Composite Coating on Ti-6Al-4V Alloy, *Opt. Laser Technol.*, 2019, **113**(October 2018), p 182-191
- L. Yang, T. Yu, M. Li, Y. Zhao, and J. Sun, Microstructure and Wear Resistance of In-Situ Synthesized Ti(C, N) Ceramic Reinforced Fe-Based Coating by Laser Cladding, *Materials Research Express*, 2019, **6**, p 8
- Z. Li, M. Wei, K. Xiao, Z. Bai, W. Xue, C. Dong, D. Wei, and X. Li, Microhardness and Wear Resistance of Al₂O₃-TiB₂-TiC Ceramic Coatings on Carbon Steel Fabricated by Laser Cladding, *Ceram. Int.*, 2018, **45**(1), p 115-121
- Z.D. Liu, X.C. Zhang, F.Z. Xuan, Z.D. Wang, and S.T. Tu, In Situ Synthesis of TiN/Ti₃Al Intermetallic Matrix Composite Coatings on Ti6Al4V Alloy, *Mater. Des.*, 2012, **37**, p 268-273
- H. Liu, X. Zhang, Y. Jiang, and R. Zhou, Microstructure and High Temperature Oxidation Resistance of In-Situ Synthesized TiN/Ti₃Al Intermetallic Composite Coatings on Ti6Al4V Alloy by Laser Cladding Process, *J. Alloys Compd.*, 2016, **670**, p 268-274
- Y. Feng, K. Feng, C. Yao, Z. Li, and J. Sun, Microstructure and Properties of In-Situ Synthesized (Ti₃Al + TiB)/Ti Composites by Laser Cladding, *Mater. Des.*, 2018, **157**(800), p 258-272
- J. Dai, N. Zhang, A. Wang, H. Zhang, and C. Chen, Microstructure and High Temperature Oxidation Behavior of Ti-Al-Nb-Si Coatings on Ti-6Al-4V Alloy, *J. Alloys Compd.*, 2018, **765**, p 46-57
- Y. Pu, B. Guo, J. Zhou, S. Zhang, H. Zhou, and J. Chen, Microstructure and Tribological Properties of in Situ Synthesized TiC, TiN, and SiC Reinforced Ti₃Al Intermetallic Matrix Composite Coatings on Pure Ti by Laser Cladding, *Appl. Surf. Sci.*, 2008, **255**, p 2697-2703
- M.M. Quazi, M.A. Fazal, A.S.M.A. Haseeb, F. Yusof, H.H. Masjuki, and A. Arslan, Effect of Rare Earth Elements and Their Oxides on Tribo-Mechanical Performance of Laser Claddings: A Review, *J. Rare Earths Chin Soc Rare Earths*, 2016, **34**(6), p 549-564
- J. Li, X. Luo, and G.J. Li, Effect of Y₂O₃ on the Sliding Wear Resistance of TiB/TiC-Reinforced Composite Coatings Fabricated by Laser Cladding, *Wear*, 2014, **310**(1–2), p 72-82
- J. Li, H. Wang, M. Li, and Z. Yu, Effect of Yttrium on Microstructure and Mechanical Properties of Laser Clad Coatings Reinforced by in Situ Synthesized TiB and TiC, *J. Rare Earths Chin. Soc. Rare Earths*, 2011, **29**(5), p 477-483
- L. Yanan, S. Ronglu, N. Wei, Z. Tiangang, and L. Yiwen, Effects of CeO₂ on Microstructure and Properties of TiC/Ti₂Ni Reinforced Ti-Based Laser Cladding Composite Coatings, *Opt. Lasers Eng.*, 2019, **120**(March), p 84-94
- Q. Li, Y. Lei, and H. Fu, Laser Cladding In-Situ NbC Particle Reinforced Fe-Based Composite Coatings with Rare Earth Oxide Addition, *Surf. Coat. Technol.*, 2014, **239**, p 102-107
- X. He, R.G. Song, and D.J. Kong, Microstructures and Properties of Ni/TiC/La₂O₃ Reinforced Al Based Composite Coatings by Laser Cladding, *Opt. Laser Technol.*, 2019, **117**(April), p 18-27
- S. Zhang, Q. Liu, L. Li, Y. Bai, and B. Yang, The Controllable Lanthanum Ion Release from Ca-P Coating Fabricated by Laser Cladding and Its Effect on Osteoclast Precursors, *Mater. Sci. Eng. C*, 2018, **93**(July 2017), p 1027-1035
- H.C. Li, D.G. Wang, C.Z. Chen, and F. Weng, Effect of CeO₂ and Y₂O₃ on Microstructure, Bioactivity and Degradability of Laser Cladding CaO-SiO₂ Coating on Titanium Alloy, *Colloids Surf. B Biointerfaces*, 2015, **127**, p 15-21
- C. Cui, X. Zhu, S. Liu, Q. Li, M. Zhang, G. Zhu, and S. Wei, Effect of Nano-Sized ZrO₂ on High Temperature Performance of Mo-ZrO₂ Alloy, *J. Alloys Compd.*, 2018, **768**, p 81-87
- B.A. Wang, N. Wang, Y.J. Yang, H. Zhong, M.Z. Ma, X.Y. Zhang, and R.P. Liu, Microstructure and Mechanical Properties of ZrO₂ Particle Dispersion Strengthened 16MnV Steel, *Mater. Sci. Eng. A*, 2017, **692**(March), p 168-173
- R.R. Behera, A. Hasan, M.R. Sankar, and L.M. Pandey, Laser Cladding with HA and Functionally Graded TiO₂-HA Precursors on Ti-6Al-4V Alloy for Enhancing Bioactivity and Cyto-Compatibility, *Surf. Coat. Technol.*, 2018, **352**, p 420-436
- Y. Cai, Y. Chen, S. Marwana, Z. Luo, F. Gao, and L. Li, Influence of Dilution Rate on the Microstructure and Properties of FeCrCoNi High-Entropy Alloy Coating, *Mater. Des.*, 2018, **142**(31), p 124-137
- D. Huang, L. Huang, B. Wang, V. Ji, and T. Zhang, The Relationship between T-ZrO₂ Stability and the Crystallization of a Zr-Based Bulk Metallic Glass during Oxidation, *Intermetallics*, 2012, **31**, p 21-25
- F. Weng, H. Yu, C. Chen, J. Liu, L. Zhao, and J. Dai, Microstructure and Property of Composite Coatings on Titanium Alloy Deposited by Laser Cladding with Co₄₂ + TiN Mixed Powders, *J. Alloys Compd.*, 2016, **686**, p 74-81
- B. Guo, J. Zhou, S. Zhang, H. Zhou, Y. Pu, and J. Chen, Phase Composition and Tribological Properties of Ti-Al Coatings Produced on Pure Ti by Laser Cladding, *Appl. Surf. Sci.*, 2007, **253**(24), p 9301-9310

33. Y. Diao and K. Zhang, Microstructure and Corrosion Resistance of TC2 Ti Alloy by Laser Cladding with Ti/TiC/TiB₂ Powders, *Appl. Surf. Sci.*, 2015, **352**, p 163-168
34. M. Zhang, S. Ma, K. Xu, L. Bai, and P.K. Chu, Bio-Tribological Properties and Cytocompatibility of Ti-Si-N Coatings, *Vacuum*, 2015, **115**, p 50-57
35. C.L. Yeh and G.S. Teng, Combustion Synthesis of TiN-TiB₂ Composites in Ti/BN/N₂ and Ti/BN/B Reaction Systems, *J. Alloys Compd.*, 2006, **424**(1–2), p 152-158
36. K. Kaviyarasu, L. Kotsedi, A. Simo, X. Fuku, G.T. Mola, J. Kennedy, and M. Maaza, Photocatalytic Activity of ZrO₂ Doped Lead Dioxide Nanocomposites: Investigation of Structural and Optical Microscopy of RhB Organic Dye, *Appl. Surf. Sci.*, 2016, **6**, p 2-7
37. F. Niu, D. Wu, G. Ma, J. Wang, M. Guo, and B. Zhang, Nano-sized Microstructure of Al₂O₃-ZrO₂(Y₂O₃) Eutectics Fabricated by Laser Engineered Net Shaping, *Scr. Mater.*, 2015, **95**(1), p 39-41
38. J. Kiilakoski, J. Puranen, E. Heinonen, H. Koivuluoto, and P. Vuoristo, Characterization of Powder-Precursor HVOF-Sprayed Al₂O₃-YSZ/ZrO₂ Coatings, *J. Therm. Spray Technol.*, 2019, **28**(1–2), p 98-107
39. A. Patra, S.K. Karak, and R. Saxena, Fabrication and Characterization of Nano-ZrO₂ Dispersed W-Based Alloy by Mechanical Alloying and Conventional Sintering, *Mater. Today Proc.*, 2017, **26**, p 3891-3902
40. N. Makuch, M. Kulka, P. Dziarski, and D. Przystacki, Laser Surface Alloying of Commercially Pure Titanium with Boron and Carbon, *Opt. Lasers Eng.*, 2014, **57**, p 64-81
41. Z. Wang, X. Zhou, and G. Zhao, Microstructure and Formation Mechanism of In-Situ TiC-TiB₂/Fe Composite Coating, *Trans. Nonferrous Met. Soc. China (English Ed.)*, 2008, **18**(4), p 831-835
42. F. Weng, H. Yu, C. Chen, and J. Dai, Microstructures and Wear Properties of Laser Cladding Co-Based Composite Coatings on Ti-6Al-4V, *Mater. Des.*, 2015, **80**, p 174-181
43. Y. Jiao, L.J. Huang, L. Geng, R. Zhang, S. Jiang, X.T. Li, and Y.N. Gao, Strengthening and Plasticity Improvement Mechanisms of Titanium Matrix Composites with Two-Scale Network Microstructure, *Powder Technology*, 2019, **356**, p 980-989

Publisher's Note Springer Nature remains neutral with regard to jurisdictional claims in published maps and institutional affiliations.